COMPUTER METHODS IN MATERIALS SCIENCE

2024, vol. 24, no. 2, 27–38
https://doi.org/10.7494/cmms.2024.2.0835

A universal convolutional neural network for the pixel-level detection and monitoring of weld beads

Zhuo Wang, Metin Kayitmazbatir, Mihaela Banu*

Department of Mechanical Engineering, University of Michigan, Ann Arbor, MI 48109, USA.

Abstract

In weld-based manufacturing processes such as welding and metal deposition additive manufacturing (AM), the weld bead is a direct indicator of manufacturing quality. For example, the geometry of the weld bead was optimized to a net shape which outperformed conventional geometries. Automatic monitoring of weld bead is thus of prime importance for welding process control and quality assurance. This paper develops a general-purpose convolutional neural network (CNN) for pixel-level detection and monitoring of beads, regardless of welding materials, machine, manufacturing conditions, etc. To achieve the generality, we collected a great variety of welding images containing 2677 single-line beads from 231 research articles, followed by pixel-wise hand-annotation. Consequently, the trained CNN can recognize different beads from various backgrounds at a pixel level. Case studies show that compared to the image-level classification in prior research, its pixel-level labeling permits real-time, complete characterization of weld beads (e.g., detailed morphology, discontinuity, spatter, and uniformity) for more informed process control. This research represents a significant step towards developing a truly human-like monitoring system with low-level scene understanding ability and general applicability.

Keywords: weld bead, additive manufacturing, machine learning, process monitoring

1. Introduction

Weld-based manufacturing processes mainly include conventional welding (DebRoy & Dawid, 1995) and various metal deposition additive manufacturing (AM), such as gas metal arc welding (GMAW) (Chaudhari et al., 2022), gas tungsten arc welding (GTAW) (Geng et al., 2017), and plasma arc welding (PAW) (Artaza et al., 2020). Those different welding processes may use different feedstock materials and energy sources, but are all characterized by the formation of weld or deposition beads (hereinafter also weld beads). A weld bead is developed upon the melting and re-solidification of feeding materials along the designated path. As the basic unit, the characteristics of the weld bead directly decide the quality of the final welding product.

To achieve high welding quality, defect-free beads with uniform geometry along the track are usually desired. However, there is a multitude of influencing factors during welding processes, leading to the easy development of irregular weld beads, such as humping (Li et al., 2016), necking (Le-Hong et al., 2021), stringing (Assunção et al., 2019), dotted and discontinuous structures (Dinovitzer et al., 2019; Zhan et al., 2016). Automatic monitoring of weld beads is thus of fundamental importance for either early process termination to minimize materials and time waste (Cho et al., 2022), or online closed-loop control after integration with process optimization modules (Wright et al., 2022; Xiong et al., 2013).

Vision-based process monitoring has been widely studied for different manufacturing processes. Some of those researchers have relied on the hand-preprocessing of

* Corresponding author: mbanu@umich.edu
ORCID ID's: 0000-0002-1657-1890 (Z. Wang), 0000-0001-6249-7938 (M. Kayitmazbatir), 0000-0002-2917-9097 (M. Banu)

as-received field images, such as Scale Invariant Feature Transform (SIFT) (Nuchitprasitchai et al., 2017) and simple threshold cutoff (Charalampous et al., 2021). The preprocessing results are then passed through analysis algorithms for final image analysis like defect detection and classification. With the advancement of machine learning (ML) techniques, especially convolutional neural networks (CNN), researchers have turned to develop CNN-based monitoring techniques with little-to-no human intervention. CNN can directly take raw field images as input and make predictions. Considerable successes have been achieved in CNN-assisted defect recognition and anomaly detection (Cho et al., 2022; Scime & Beuth, 2018; Zhang et al., 2019). However, existing CNN approaches still have two major limitations. Firstly, they usually focus on high-level prediction by simply outputting a category or label about the entire image, i.e., image classification. Therefore, the monitoring system lacks a detailed understanding of field images, which is however critically demanded for more informed decision-making and process control. Secondly, CNNs are trained for a specific manufacturing process or machine, while without applicability to others. This considerably limits the practical usage of the trained monitoring system beyond their respective in-house machine.

To address the above-mentioned gap, this paper presents a universal CNN for pixel-level understanding of different weld bead images. A large number of weld bead images for varied welding processes are first collected from the literature, followed by pixel-wise manual annotation yielding the segmentation images. We thus create an image-to-image pairing datasets with great variability, which is the first of its kind for the manufacturing process. It enables CNN to learn and then automatically recognize the bead region at a pixel level. Consequently, the trained CNN permits real-time and complete characterization of the bead structure and morphology, by which many bead properties (e.g., discontinuity, spatter, uniformity, and even detailed geometrical deviation) can be further derived for well-informed process control. It opens possibilities for developing human-like monitoring systems capable of fully understanding field images and, more importantly, applicable to general welding processes.

2. Method

2.1. Weld bead image dataset

The availability of dataset plays a pivotal role in the wide adoption and increasing success of machine learning (ML) in various domains nowadays. Computer scientists have pointed out that, the learning algorithms reaching human performance on complex tasks today are nearly identical to the learning algorithms that struggled to solve toy problems in the 1980s (LeCun et al., 2015). The most important new development is that today we can provide these algorithms with the resources they need to succeed. With the increasing availability of digital data, big data or data deluge is arguably one of the most important factors that drives the success of machine learning in various fields nowadays. Motivated by the attempts of leveraging big literature data in different domains (Wang et al., 2022a), here we create the first welding dataset for image segmentation purposes to further realize the tremendous potential of ML in welding process monitoring and control.

As illustrated in Figure 1, different weld bead images are first gathered from 231 research papers, where different welding machines, manufacturing conditions and even imaging techniques have been used. Consequently, we get a total of 2677 single-pass beads, featuring a great variety of bead morphology, texture, contrast to surroundings, and so on[1]. The great diversity of weld bead images is critical to training a robust ML model applicable to different weld-based processes. Among them, 2045 beads are used for training and validation, and 632 beads for testing. After the image data collection, we manually label images in a pixel-wise manner, i.e., delineating the weld bead region from the background. To build a dataset without unnecessary noise and with maximum variety, we cut off the blank margin for as-collected images. However, some other types of noise, such as arrows and label text possibly contained in the images are kept, since they are difficult to remove precisely. On the other hand, appropriate noise is expected to improve the robustness of the trained CNN. Note that, there are also some images that contain indistinguishable weld beads. Their profiles are not well recognized even for human labelers due to blurry images or simply bad lighting conditions during imaging. We keep those images in our dataset, and label them with our best efforts. Following manual labeling, we properly resize those images since they may have rather different resolutions and different densities of tracks. For the training dataset, each image is further cropped into small images with a predefined resolution (here 128 × 128 pixels) to facilitate training, as CNN prefers accepting images of fixed size during training. Therefore, the foregoing resizing operation is strictly performed so that the cropped image would generally contain 2–3 tracks with enough background. We posit that by doing so, CNN can best learn to distinguish bead tracks from various backgrounds. Eventually, after the two-step data preprocessing, the original training and validation dataset yields 6482 patches with a fixed resolution of 128 × 128.

[1] The full dataset can be accessed at: https://data.mendeley.com/datasets/9mrmttnjh5/1.

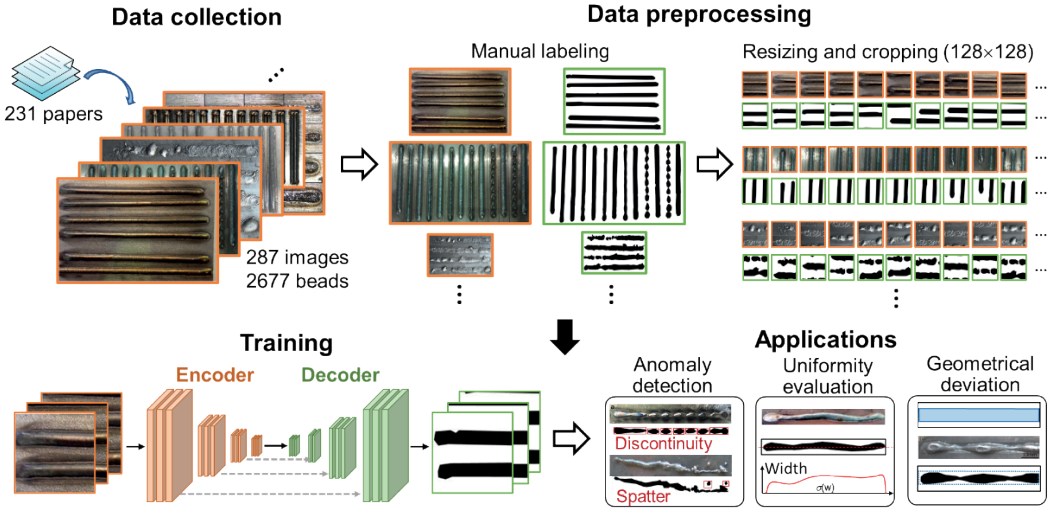

Fig. 1. Graphical illustration of developing a general-purpose CNN for pixel-level bead detection and monitoring based on high-volume bead image data in literature

2.2. Fully convolutional neural network for image segmentation

As shown in Figure 1, a fully convolutional encoder-decoder CNN is built based on U-Net originally intended for biomedical image segmentation (Ronneberger et al., 2015). We choose U-Net as the basis CNN because of its ease of implementation with a neat architecture and well-demonstrated reliability in image segmentation. Additionally, its fully convolutional architecture allows for taking input images of variable size during prediction (Wang et al., 2022b). This feature is especially valuable for bead recognition, since bead of variable length and width is a common practice across different weld-based manufacturing processes, as demonstrated later in testing. We properly adjust the depth and width of the original U-Net, as well as adding a dropout layer to avoid overfitting. Table 1 gives the detailed architecture of the implemented CNN for bead image segmentation. The above CNN is then trained with the image-to-image pairing dataset as described in the last subsection, and the cross-entropy loss function is adopted to properly penalize predictive inaccuracy in a (pixel-wise) classification task (Kohler & Langer, 2020). We trained it for 300 epochs using a batch size of 32. Figure 2 presents the learning curve during the training process. CNN achieves a minimal validation loss of 0.0456 at the 247th epoch, where its weights are saved and used for prediction in the remainder of the paper.

The trained CNN can be used in many applications depending on the monitoring and control objectives. It can detect the detailed bead morphology and structure, which would yield rich information about the weld bead. For example, continuity/discontinuity of a weld bead can be judged based on the number of self-connected bead regions upon image segmentation. The geometrical characteristics of discrete beads (e.g., size, shape, and variation) can be further determined, which can indicate the specific cause of the discontinuity for informing more precise process control. The uniformity of the weld bead can also be quickly evaluated by simply calculating the width for the entire detected bead. It gives an instantaneous, quantitative, and objective evaluation of bead quality, which is otherwise too laborious by hand measurement. The deviation of the weld building from the designed geometry and location can also be decided, as the CNN gives the detailed profile of the bead region. In summary, due to its pixel-level understanding of the field images, the trained CNN opens possibilities for weld process monitoring and control with unprecedented flexibility and accuracy, as demonstrated in the following section.

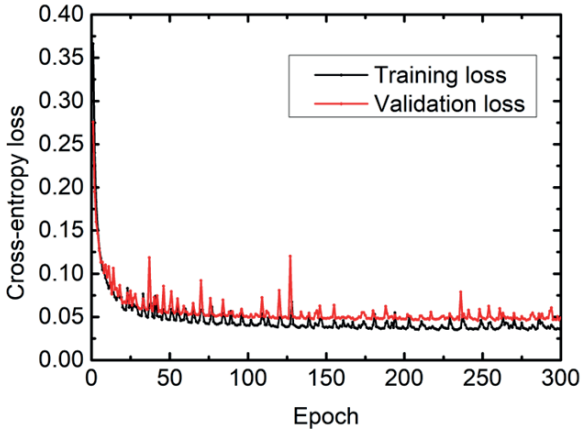

Fig. 2. Learning curve during training the fully convolutional CNN for image segmentation of weld bead images

Table 1. Architecture of the adopted CNN for bead image segmentation

Layer name		Output shape
Encoder	Input	(128, 128, 3)
	Block1_conv1	(128, 128, 16)
	Block1_conv2	(128, 128, 16)
	Block1_pool	(64, 64, 16)
	Block2_conv1	(64, 64, 32)
	Block2_conv2	(64, 64, 32)
	Block2_pool	(32, 32, 32)
	Block3_conv1	(32, 32, 64)
	Block3_conv2	(32, 32, 64)
	Block3_pool	(16, 16, 64)
	Block4_conv1	(16, 16, 128)
	Block4_conv2	(16, 16, 128)
	Block4_drop	(16, 16, 128)
	Block4_pool	(8, 8, 128)
	Block5_conv1	(8, 8, 256)
	Block5_conv2	(8, 8, 256)
	Block5_drop	(8, 8, 256)
Decoder	Block6_upsampling	(16, 16, 256)
	Block6_conv1	(16, 16, 128)
	Block6_concatenate	(16, 16, 256)
	Block6_conv2	(16, 16,128)
	Block6_conv3	(16, 16, 128)
	Block7_upsampling	(32, 32, 128)
	Block7_conv1	(32, 32, 64)
	Block7_concatenate	(32, 32, 128)
	Block7_conv2	(32, 32, 64)
	Block7_conv3	(32, 32, 64)
	Block8_upsampling	(64, 64, 64)
	Block8_conv1	(64, 64, 32)
	Block8_concatenate	(64, 64, 64)
	Block8_conv2	(64, 64, 32)
	Block8_conv3	(64, 64, 32)
	Block9_upsampling	(128, 128, 32)
	Block9_conv1	(128, 128, 16)
	Block9_concatenate	(128, 128, 32)
	Block9_conv2	(128, 128, 16)
	Block9_conv3	(128, 128, 16)
	Block9_conv4	(128, 128, 2)
	Output	(128, 128, 1)

2.3. Additively manufactured deposition beads

In order for our testing dataset to be more complete, we performed several deposition experiments using our own laser directed energy deposition setup. Both the baseplate and stock material were 7075 Aluminum alloy to reduce visual variation. While most of the input parameters were kept constant, only the laser power was changed in 200 watt increments. Deposited beads were cleaned with compressed air and a metal brush to get rid of loose particles and final photos were shown in Figure 2c. Process parameters which were used are: power 1000–2000 W with a 200 increment, 1 mm laser beam diameter, 3.81 mm/s scanning speed, 0.02 g/m powder deposition rate, Argon with a 30 standard cubic feet of gas per hour as shielding and delivery gas.

3. Results and discussions

3.1. Pixel-level detection of bead morphology

We first apply the trained CNN for identifying the morphology of different testing beads unused in training and validation. For full testing, the testing dataset further includes a few samples fabricated in our lab, as shown in Figure 3c. Instead of taking small square patches as input during training, CNN is now fed with the entire image of long beads to clearly show its predictive performance. Figure 3 presents some representative testing results. It can be found that in general, the trained CNN can correctly identify beads from different backgrounds. Noteworthy is that the testing image in Figure 3c contains various types of noise, with some interfering with the track (e.g., the red dotted line). They present further challenges for identifying the slim beads therein, but the trained CNN still performs reasonable segmentation. In addition to qualitative examination, we calculate the pixel-wise global accuracy, i.e., the percentage of correctly classified pixels. The trained CNN achieves a high global accuracy of 84.15% on average for all 632 testing tracks.

However, it should be pointed out that predictive errors take place under some special circumstances. For example, testing results indicate that CNN always struggles to identify beads in shadows. CNN can recognize the whole shadow region as either background (Fig. 3a) or bead (Fig. 3d). It emphasizes the importance of good lighting for reliable bead detection. Type-1 errors in Figure 3b and d imply that those non-bead regions with bead-like color and texture frequently confuse CNN. There are also other types of predictive errors that happen for less well-known reasons. For instance, the type-2 error in Figure 3d shows that CNN suddenly predicts wrongly in the middle of the long bead, which however shows quite a constant appearance along its length. With the ever-accumulating training data and rapid advancement of ML algorithms, those different predictive errors are anticipated to be alleviated or even corrected in the future.

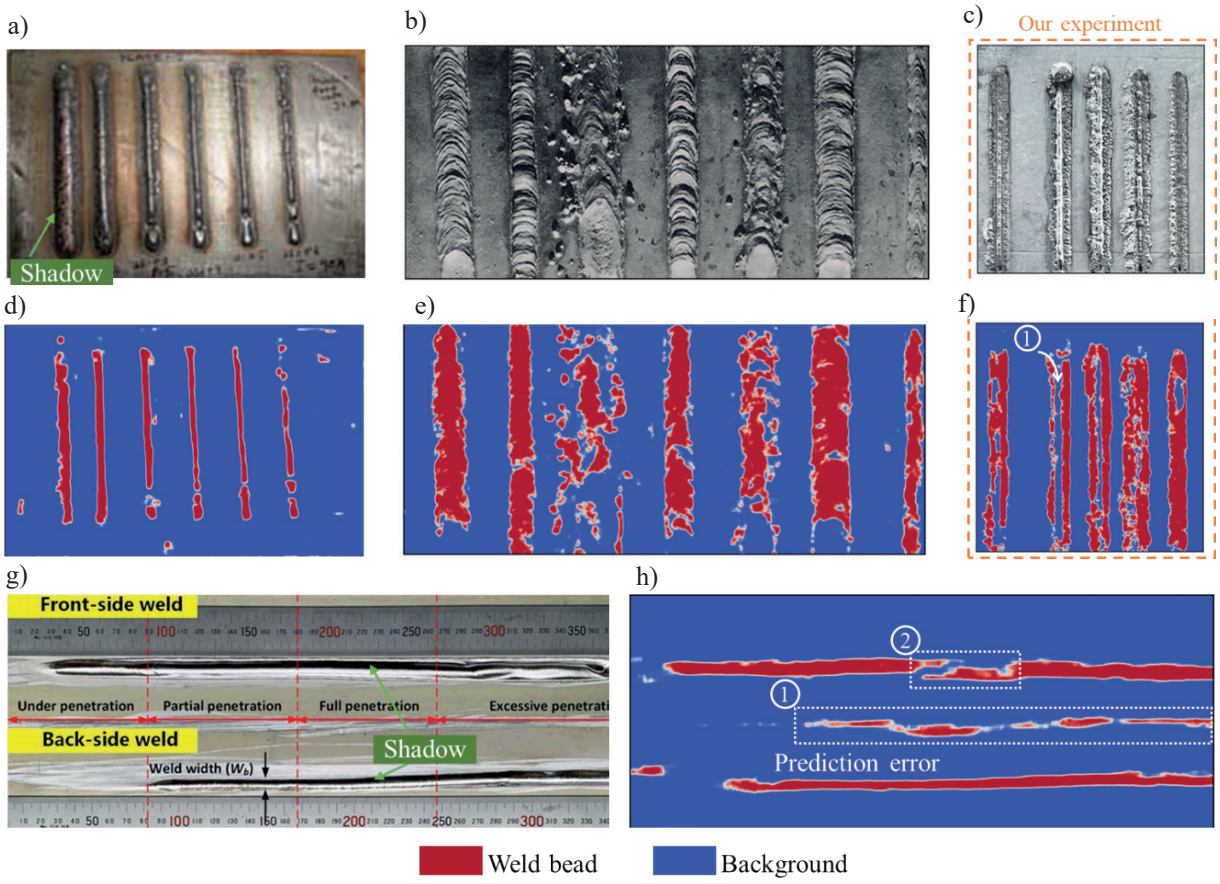

Fig. 3. Testing of the trained CNN on identifying different beads from various background; a) set 1 of experimental beads by Mandal et al. (2015); b) set 2 of experimental weld beads by Althouse et al. (2004) and Wu et al. 2021; c) set 3 of experimental beads obtained through directed-energy deposition at the University of Michigan; d) CNN prediction of the beads shape and defects from Fig. 3a; e) CNN prediction of the beads shape and defects from Fig. 3b; f) CNN prediction of the beads shape and defects from Fig. 3c; g) subset of experimental set 3 showing three beads with different level of shadows; h) CNN prediction of the shape and defects including shadows

3.2. Automatic monitoring of bead anomaly: discontinuity and spatter

Upon the image segmentation by CNN, more actionable information can be quickly derived to guide the welding process control. We first show the automatic detection of bead discontinuity by further processing the raw segmentation result. In welding process, bead discontinuity is a common issue, especially in pursuit of high productivity by increasing the travel speed of the welding torch. To detect the discontinuity, we propose to calculate the number of self-connected bead regions in the segmentation image. As shown in Figure 4a, a total of 15 isolated bead regions (also known as balling effect) are detected for the testing track. The number of detected bead regions indicates the discontinuity, i.e., 1 for full continuity and others for discontinuity. Instead of delivering a binary classification (continuous or discontinuous), the current CNN further tells the discontinuity level reflected by the total number of discrete beads. In fact, the CNN with accurate image segmentation give the complete discontinuity-related information, such as size, spacing or density of discrete beads; see Figure 4b. This information is useful as quantitative feedback for properly adjusting welding parameters, such as the traveling speed of the welding torch and the feeding rate of welding material. These details about discontinuity were previously unobtainable based on an image classification CNN.

Another typical type of bead irregularity is spatter. It can result from intensive heat dissipation to the atmosphere and associated splash of metal flux transferred to the molten pool (Jamrozik & Górka, 2020), or overheating and explosion of welding materials (Meng et al., 2018). The monitoring system can detect the spatter behavior using a similar postprocessing algorithm, namely inspecting the number of discrete bead regions, since the spatter would generally present as many small scattered bead regions; see Figure 5a. For the monitoring system to further distinguish spatter from discontinuity, we also implement another numerical algorithm to analyze the spatial distribution of discrete bead regions in the transverse direction, based on their centroid information as shown in Figure 5b. Figure 5c compares the distribution patterns in spatter and discontinuity situations. It can be seen that in the spatter case, small bead regions are widely distributed around the main bead with a significantly larger size, while the discontinuity is characterized with a line of closely aligned discrete beads with similar sizes along the track. Therefore, after detecting the existence of discrete beads, their statistical characteristics (e.g., variance of location in the transverse direction and variance of bead size) can be further used to decide whether spatter or discontinuity occurs.

a)

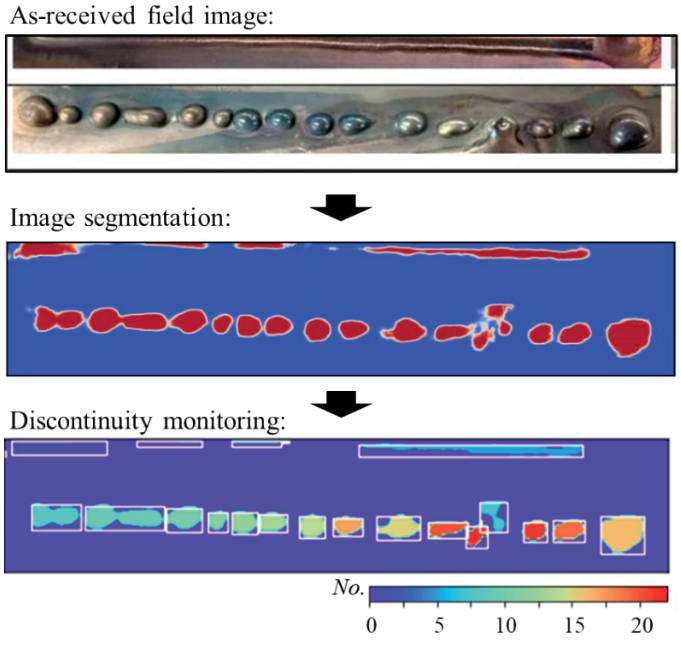

b)

No.	Shape	Area (px²)	(x_0, y_0)
1		400	(71.45, 471.97)
2		771	(73.70, 47.75)
3		1205	(75.30, 112.96)
4		572	(75.45, 174.53)
5		261	(77.93, 205.98)
6		416	(80.17, 231.20)
7		382	(79.88, 259.02)
8		437	(83.87, 297.24)
9		616	(85.06, 381.82)
10		1173	(90.12, 596.16)
11		388	(83.10, 331.19)
12		465	(87.83, 544.17)
13		415	(85.90, 426.53)
14		349	(88.04, 511.57)
15		267	(92.52, 455.58)

Fig. 4. The trained CNN can be applied to monitor the continuity of bead based on the number of detected (discrete) beads (a) and the detailed information of each discrete bead is obtainable as quantitative feedback for process adjustment (b). The testing image is taken from the experiment in the work by Cho et al. (2022)

a)

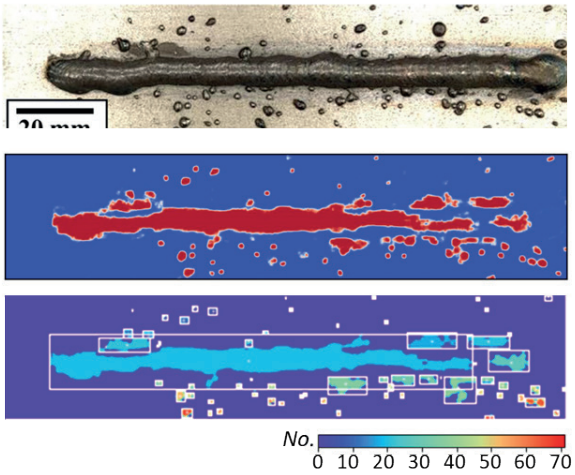

b)

No.	Shape	(x_0, y_0)
1		(9.57, 973.48)
2		(58.21, 785.59)
3		(82.06, 297.86)
4		(105.30, 253.03)
5		(175.50, 821.10)
6		(192.80, 933.04)
7		(185.22 701.88)
8		(187.68, 483.92)
…	…	…

c)

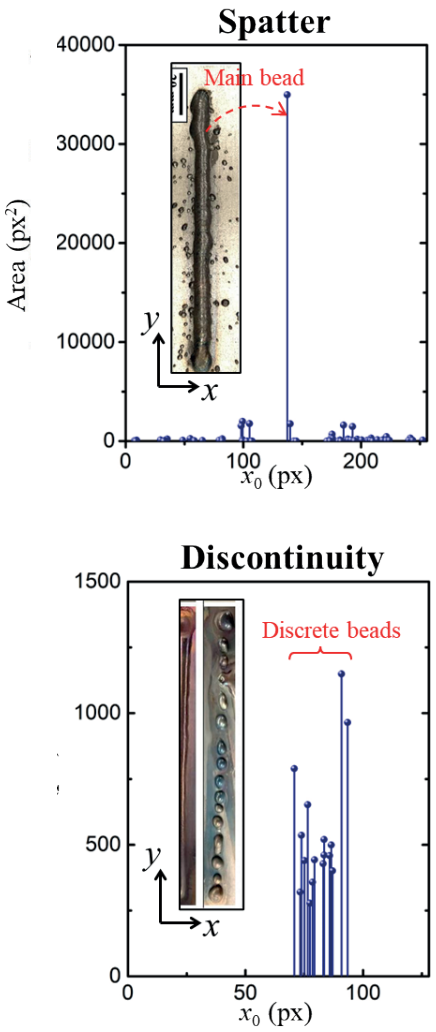

Fig. 5. The trained CNN is applicable to monitoring spatter of bead based on the detected bead regions showing scattered distribution (a); the centroid information of detected bead regions (b); comparison of the distribution of detected bead regions in transverse direction between bead spatter and discontinuity (c). The spatter image is taken from the experiment in the work by Lee et al. (2022)

3.3. Quick evaluation of bead uniformity

Bead nonuniformity is a severe problem in the welding process, especially at the arc onset and extinguishing stages which are known for their process instability and poor controllability (Tang et al., 2020). In addition, the humping phenomenon concerned with strong backward melt flow and capillary instability is widely observed, leading to periodic undulation of the entire weld bead (Yuan et al., 2020). To evaluate the bead uniformity, we propose a postprocessing algorithm to count the number of pixels contained in the detected bead region in the transverse direction. Figure 6a displays the two testing weld beads and their raw image segmentation results by the trained CNN. Visual inspection reveals the clear bead nonuniformity by the bulgy arc striking region for the second weld bead. Figure 6b shows the quantitative evaluation of uniformity by using the aforementioned algorithm, as well as the ground truth by manual measurement. The proposed algorithm easily computes the width for the entire weld bead, and generates the detailed variation of width along its length that matches well with the ground truth. Based on the computation results, a variance of width is further calculated, quantitatively indicative of the bead nonuniformity, i.e., $\sigma = 2.5$ pixels and $\sigma = 7.9$ pixels for the first and second testing track, respectively.

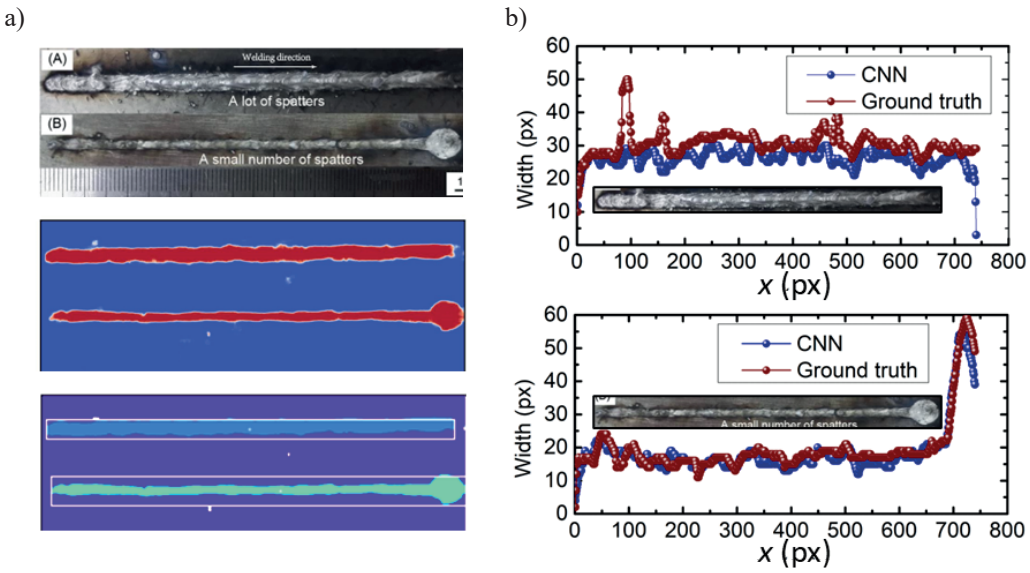

Fig. 6. The trained CNN can be applied to monitor the uniformity of the weld bead by quickly calculating the width along the entire bead: a) raw segmentation results and the two detected weld beads; b) postprocessing results of bead width variation for evaluating uniformity of weld bead. The testing image is taken from the experiment in the work by Wu et al. (2017)

3.4. Applicability to multi-track beads

In this subsection, we test the as-trained CNN on identifying multi-track and complex beads from its background. The testing examines the applicability of as-trained CNN far beyond the training data of single-line beads. It is meaningful for some applications where recognizing the bulk in-plane geometry of the weld building is a necessity, e.g., detection of the geometrical deviation from the designed shape (Ruiz et al., 2022). For instance, direct metal deposition, although possessing a high building rate compared to powder-bed-based AM, is criticized for its low geometric precision (Jafari et al., 2021). Therefore, there is an urgent need for the automated capability of detecting geometrical errors during metal deposition AM. Figure 7 shows testing results with respect to three rather different complex weld buildings. The welding components in Figure 7a and b are basically interconnected single-line beads, while the one in Figure 7c is made of tightly overlapped beads. It can be found that misclassification of bead-like background as bead region still exists in the multi-track case, as indicated by type-1 error in Figure 7a. Type-2 error in Figure 7b shows that CNN often performs the wrong prediction for junction areas. This can possibly be attributed to the absence of such bead features in the training dataset of single-line beads. The same is true for the testing welding building in Figure 7c, as reflected by type-3 error. CNN fails to recognize the entirety of overlapped beads as bead regions, because the current training dataset contains only single-track beads without overlapping textures.

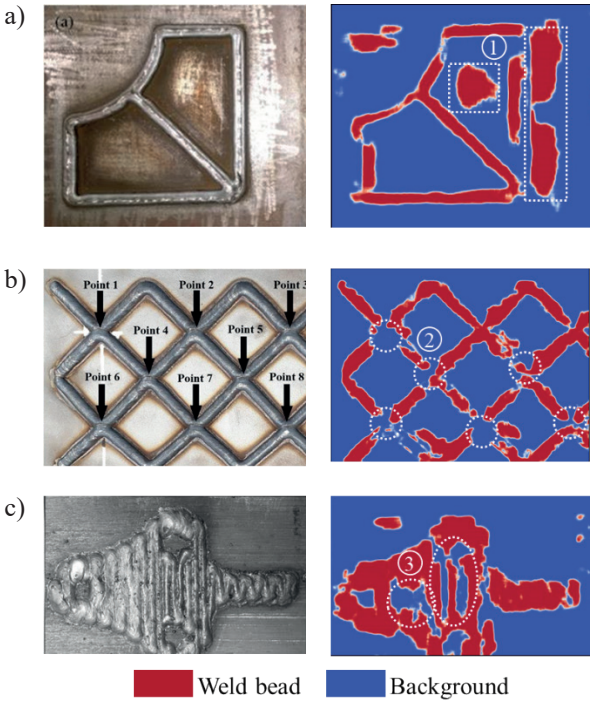

Fig. 7. Testing of the trained CNN on identifying multi-track and complex beads: a) interconnected beads; b) interconnected beads; c) overlapped beads. The testing images are taken from experiments in works by Ding et al. (2015); Song et al. (2021); Sreenathbabu et al. (2005)

Thus, bead features completely out of the training dataset severely challenge the as-trained CNN. Nonetheless, except in those special situations, the overall prediction is reasonable in all three testing cases. The testing thus demonstrates the useful knowledge in the

single-track dataset for the CNN to recognize multi-track beads. A robust CNN for detecting multi-track beads might be trained by fine-tuning the current CNN using a small dataset of multi-track beads (i.e., transfer learning (Wang et al., 2022a)) in the near future. This is valuable considering the high cost of fabricating and manually labeling multi-track weld buildings.

4. Conclusion

An automated process monitoring system with human-level scene understanding ability has long been pursued in the manufacturing community. In this paper, we trained a CNN for pixel-level field image segmentation, and with applicability to different welding processes. In addition, different postprocessing algorithms are proposed and tested for converting raw segmentation results to actionable information, namely existence, severity level, and other quantitative details of different bead irregularities. This would allow for weld process monitoring and control with unprecedented flexibility and accuracy. Therefore, the proposed CNN, together with those postprocessing algorithms, forms a prototype towards developing the long-pursued process monitoring system with truly human-like performance. Concluding remarks are made as below:

- The CNN trained on high-volume bead images in the literature can identify bead regions from various backgrounds, achieving a global accuracy of 84.15%. Predictive errors mainly occur for some bead parts in the shadows and background with bead-like texture.
- Upon image segmentation, the monitoring system can detect the bead discontinuity and spatter, by calculating the number of connected bead regions and further analyzing their statistical characteristics.
- The monitoring system can quickly evaluate the bead uniformity by computing the width along the entire bead based on the segmentation result.
- The as-trained CNN predict reasonably well for multi-track and complex beads. It indicates the possibility of economically developing a CNN for detecting the bulk geometry of large weld buildings by fine-tuning using a small dataset of multi-track beads.

Acknowledgements

The authors acknowledge the funding support from M-Cubed Program at the University of Michigan, START Program at the College of Engineering at the University of Michigan and the DOE Project DE-EE0009402.

Contributions

Z.W. and M.B. conceived the idea and designed the research. Z.W. and M.K. collected and hand-annotated the weld bead images in the literature. M.K. conducted the direct energy deposition experiments. Z.W. developed and trained the CNN, and wrote the paper under the supervision of M.B. All authors reviewed and approved the manuscript.

Declaration of competing interest

The authors declare no known competing financial interests or personal relationships that could have appeared to influence the work reported in this paper.

References

Althouse, A. D., Turnquist, C. H., Bowditch, W. A., Bowditch, K. E., & Bowditch, M. A. (2004). *Modern welding*. Goodheart-Wilcox.

Artaza, T., Suárez, A., Veiga, F., Braceras, I., Tabernero, I., Larrañaga, O., & Lamikiz, A. (2020). Wire arc additive manufacturing Ti6Al4V aeronautical parts using plasma arc welding: Analysis of heat-treatment processes in different atmospheres. *Journal of Materials Research and Technology*, *9*(6), 15454–15466. https://doi.org/10.1016/j.jmrt.2020.11.012.

Assunção, P. D. C., Ribeiro, R. A., Dos Santos, E. B. F., Braga, E. M., & Gerlich, A. P. (2019). Comparing CW-GMAW in direct current electrode positive (DCEP) and direct current electrode negative (DCEN). *The International Journal of Advanced Manufacturing Technology*, *104*, 2899–2910. https://doi.org/10.1007/s00170-019-04175-2.

Charalampous, P., Kostavelis, I., Kopsacheilis, C., & Tzovaras, D. (2021). Vision-based real-time monitoring of extrusion additive manufacturing processes for automatic manufacturing error detection. *The International Journal of Advanced Manufacturing Technology*, *115*, 3859–3872. https://doi.org/10.1007/s00170-021-07419-2.

Chaudhari, R., Parmar, H., Vora, J., & Patel, V. K. (2022). Parametric study and investigations of bead geometries of GMAW-based wire–arc additive manufacturing of 316L stainless steels. *Metals*, *12*(7), 1232. https://doi.org/10.3390/met12071232.

Cho, H.-W., Shin, S.-J., Seo, G.-J., Kim, D. B., & Lee, D.-H. (2022). Real-time anomaly detection using convolutional neural network in wire arc additive manufacturing: Molybdenum material. *Journal of Materials Processing Technology*, *302*, 117495. https://doi.org/10.1016/j.jmatprotec.2022.117495.

DebRoy, T., & David, S. (1995). Physical processes in fusion welding. *Reviews of Modern Physics*, *67*(1), 85–112. https://doi.org/10.1103/RevModPhys.67.85.

Ding, D., Pan, Z., Cuiuri, D., & Li, H. (2015). A practical path planning methodology for wire and arc additive manufacturing of thin-walled structures. *Robotics and Computer-Integrated Manufacturing*, *34*, 8–19. https://doi.org/10.1016/j.rcim.2015.01.003.

Dinovitzer, M., Chen, X., Laliberte, J., Huang, X., & Frei, H. (2019). Effect of wire and arc additive manufacturing (WAAM) process parameters on bead geometry and microstructure. *Additive Manufacturing*, *26*, 138–146. https://doi.org/10.1016/j.addma.2018.12.013.

Geng, H., Li, J., Xiong, J., Lin, X., & Zhang, F. (2017). Optimization of wire feed for GTAW based additive manufacturing. *Journal of Materials Processing Technology*, *243*, 40–47. https://doi.org/10.1016/j.jmatprotec.2016.11.027.

Jafari, D., Vaneker, T. H. J., & Gibson, I. (2021). Wire and arc additive manufacturing: Opportunities and challenges to control the quality and accuracy of manufactured parts. *Materials & Design*, *202*, 109471. https://doi.org/10.1016/j.matdes.2021.109471.

Jamrozik, W., & Górka, J. (2020). Assessing MMA welding process stability using machine vision-based arc features tracking system. *Sensors*, *21*(1), 84. https://doi.org/10.3390/s21010084.

Kohler, M., & Langer, S. (2020). *Statistical theory for image classification using deep convolutional neural networks with cross-entropy loss*. arXiv. https://doi.org/10.48550/arXiv.2011.13602.

LeCun, Y., Bengio, Y., & Hinton, G. (2015). Deep learning. *Nature*, 521(7553), 436–444.

Lee, T. H., Kim, Ch., Oh, J. H., & Kam, D. H. (2022). Visualization of cathode spot control using laser irradiation and oxide addition in wire arc additive manufacturing of titanium alloys. *Journal of Laser Applications*, *34*(4), 042024. https://doi.org/10.2351/7.0000738.

Le-Hong, T., Lin, P. C., Chen, J.-Z., Pham, T. D. Q., & Van Tran, X. (2021). Data-driven models for predictions of geometric characteristics of bead fabricated by selective laser melting. *Journal of Intelligent Manufacturing*, *34*, 1241–1257. https://doi.org/10.1007/s10845-021-01845-5.

Li, Y., Wu, C., Wang, L., & Gao, J. (2016). Analysis of additional electromagnetic force for mitigating the humping bead in high-speed gas metal arc welding. *Journal of Materials Processing Technology*, *229*, 207–215. https://doi.org/10.1016/j.jmatprotec.2015.09.014.

Mandal, S., Kumar, S., Bhargava, P., Premsingh, C., Paul, C. P., & Kukreja, L. M. (2015). An experimental investigation and analysis of PTAW process. *Materials and Manufacturing Processes*, *30*(9), 1131–1137. https://doi.org/10.1080/10426914.2014.984227.

Meng, Y., Gao, M., & Zeng, X. (2018). Quantitative analysis of synergic effects during laser-arc hybrid welding of AZ31 magnesium alloy. *Optics and Lasers in Engineering*, *111*, 183–192. https://doi.org/10.1016/j.optlaseng.2018.08.013.

Nuchitprasitchai, S., Roggemann, M. C., & Pearce, J. M. (2017). Three hundred and sixty degree real-time monitoring of 3-D printing using computer analysis of two camera views. *Journal of Manufacturing and Materials Processing*, *1*(1), 2. https://doi.org/10.3390/jmmp1010002.

Ronneberger, O., Fischer, P., & Brox, T. (2015). U-net: Convolutional networks for biomedical image segmentation. In *Medical Image Computing and Computer-Assisted Intervention – MICCAI 2015. 18th International Conference, Munich, Germany, October 5–9, 2015, Proceedings* (pt. III, pp. 234–241). Springer Cham. https://doi.org/10.1007/978-3-319-24574-4_28.

Ruiz, C., Jafari, D., Subramanian, V. V., Vaneker, T. H. J., Ya, W., & Huang, Q. (2022). Prediction and control of product shape quality for wire and arc additive manufacturing. *Journal of Manufacturing Science and Engineering*, *144*(11), 111005. https://doi.org/10.1115/1.4054721.

Scime, L., & Beuth, J. (2018). A multi-scale convolutional neural network for autonomous anomaly detection and classification in a laser powder bed fusion additive manufacturing process. *Additive Manufacturing*, *24*, 273–286. https://doi.org/10.1016/j.addma.2018.09.034.

Song, G.-H., Lee, C.-M., & Kim, D.-H. (2021). Investigation of path planning to reduce height errors of intersection parts in wire-arc additive manufacturing. *Materials*, *14*, 6477. https://doi.org/10.3390%2Fma14216477.

Sreenathbabu, A., Karunakaran, K., & Amarnath, C. (2005). Statistical process design for hybrid adaptive layer manufacturing. *Rapid Prototyping Journal*, *11*(4), 235–248. https://doi.org/10.1108/13552540510612929.

Tang, S., Wang, G., Huang, C., Li, R., Zhou, S., & Zhang, H. (2020). Investigation, modeling and optimization of abnormal areas of weld beads in wire and arc additive manufacturing. *Rapid Prototyping Journal*, *26*(7), 1183–1195. https://doi.org/10.1108/RPJ-08-2019-0229.

Wang, Z., Yang, W., Liu, Q., Zhao, Y., Liu, P., Wu, D., Banu, M., & Chen, L. (2022a). Data-driven modeling of process, structure and property in additive manufacturing: A review and future directions. *Journal of Manufacturing Processes*, *77*, 13–31. https://doi.org/10.1016/j.jmapro.2022.02.053.

Wang, Z., Yang, W., Xiang, L., Wang, X., Zhao, Y., Xiao, Y., Liu, P., Liu, Y., Banu, M., Zikanov, O., & Chen, L. (2022b). Multi-input convolutional network for ultrafast simulation of field evolvement. *Patterns*, *3*(6), 100494. https://doi.org/10.1016/j.patter.2022.100494.

Wright, W. J., Darville, J., Celik, N., Koerner, H., & Celik, E. (2022). In-situ optimization of thermoset composite additive manufacturing via deep learning and computer vision. *Additive Manufacturing*, *58*, 102985. https://doi.org/10.1016/j.addma.2022.102985.

Wu, D., Hua, X., Li, F., & Huang, L. (2017). Understanding of spatter formation in fiber laser welding of 5083 aluminum alloy. *International Journal of Heat and Mass Transfer*, *113*, 730–740. https://doi.org/10.1016/j.ijheatmasstransfer.2017.05.125.

Wu, D., Hu, M., Huang, Y., Zhang, P., & Yu, Z. (2021). *In situ* monitoring and penetration prediction of plasma arc welding based on welder intelligence-enhanced deep random forest fusion. *Journal of Manufacturing Processes*, *66*, 153–165. https://doi.org/10.1016/j.jmapro.2021.04.007.

Xiong, J., Zhang, G., Qiu, Z., & Li, Y. (2013). Vision-sensing and bead width control of a single-bead multi-layer part: Material and energy savings in GMAW-based rapid manufacturing. *Journal of Cleaner Production*, *41*, 82–88. https://doi.org/10.1016/j.jclepro.2012.10.009.

Yuan, L., Pan, Z., Ding, D., He, F., Duin, S. van, Li, H., & Li, W. (2020). Investigation of humping phenomenon for the multi-directional robotic wire and arc additive manufacturing. *Robotics and Computer-Integrated Manufacturing*, *63*, 101916. https://doi.org/10.1016/j.rcim.2019.101916.

Zhang, Z., Wen, G., & Chen, S. (2019). Weld image deep learning-based on-line defects detection using convolutional neural networks for Al alloy in robotic arc welding. *Journal of Manufacturing Processes*, *45*, 208–216. https://doi.org/10.1016/j.jmapro.2019.06.023.